



# CHORUS

This is the accepted manuscript made available via CHORUS. The article has been published as:

## Commensurate and incommensurate spin-density waves and the superconductivity dome in heavy electron systems

P. Schlottmann

Phys. Rev. B **92**, 045115 — Published 16 July 2015

DOI: [10.1103/PhysRevB.92.045115](https://doi.org/10.1103/PhysRevB.92.045115)

# Commensurate and incommensurate spin-density waves and the superconductivity dome in heavy electron systems

P. Schlottmann

*Department of Physics, Florida State University, Tallahassee, Florida 32306*

The nesting of the Fermi surfaces of an electron and a hole pocket separated by a nesting vector  $\mathbf{Q}$  and the interaction between electrons gives rise to itinerant antiferromagnetism. The order can gradually be suppressed by mismatching the nesting and a quantum critical point is obtained as the Néel temperature tends to zero. If the vector  $\mathbf{Q}$  is commensurate with the lattice (Umklapp with  $\mathbf{Q} = \mathbf{G}/2$ ), pairs of electrons can be transferred between the pockets and a superconducting dome above the quantum critical point may arise. If the vector  $\mathbf{Q}$  is not commensurate with the lattice there are eight phases that need to be considered: commensurate and incommensurate spin and charge density waves and four superconductivity phases, two of them with modulated order parameter of the FFLO type. The renormalization group equations are studied and numerically integrated. The phase diagram is obtained as a function of the mismatch of the Fermi surfaces and the magnitude of  $|\mathbf{Q} - \mathbf{G}/2|$ .

PACS numbers: 71.27.+a, 71.28.+d, 72.15.Qm, 75.20.Hr

## I. INTRODUCTION

Landau's Fermi liquid (FL) theory has been successful in describing the low energy properties of most normal metals. However, numerous heavy fermion systems<sup>1-4</sup> display deviations from FL behavior, known as non-Fermi liquid (NFL) properties. NFL manifests itself as, e.g., a  $\log(T)$ -dependence in the specific heat over  $T$ , a singular behavior at low  $T$  of the magnetic susceptibility, and a power-law dependence of the resistivity, with an exponent close to one. This breakdown of the FL can be tuned by alloying (chemical pressure), hydrostatic pressure or the magnetic field. In most cases the systems are close to the onset of antiferromagnetism (AF) and the NFL behavior is attributed to a quantum critical point (QCP).<sup>5-15</sup> NFL behavior, AF order and a superconducting dome in the neighborhood of a QCP have been observed in  $\text{CeRh}_2\text{Si}_2$ ,<sup>16,17</sup>  $\text{CePd}_2\text{Si}_2$  and  $\text{CeIn}_3$ <sup>18,19</sup> under pressure.

Previously, we have studied the pre-critical region of a heavy electron band with two parabolic pockets, one electron-like and the other hole-like, separated by a wave vector  $\mathbf{Q}$ . The interaction is the remaining repulsion between heavy quasiparticles after the heavy particles have been formed in the sense of a Fermi liquid and is assumed to be weak. If the number of particles in each pocket is conserved the interaction consists of three terms: (i) a small momentum transfer between the pockets,  $V(\mathbf{q})$ , (ii) a large momentum transfer between the pockets of the order of  $\mathbf{Q}$ ,  $U$ , and (iii) an interaction between quasiparticles in the same pocket,  $W$ . We used (1) a field-theoretical multiplicative renormalization group (RG) approach<sup>10</sup> and (2) the Wilsonian RG<sup>20</sup> that eliminate the fast degrees of freedom close to an ultraviolet cutoff and rewrite the Hamiltonian in terms of renormalized slow variables.<sup>13</sup> The interaction  $V$  induces itinerant AF due to the nesting of the Fermi surfaces of the two pockets. For perfect nesting (electron-hole symmetry

between the pockets) an arbitrarily small interaction is sufficient for a ground state with long-range order. The degree of nesting is controlled by the mismatch parameter,  $\delta = \frac{1}{2}|k_{F1} - k_{F2}|v_F$ , where  $k_{F1}$  ( $k_{F2}$ ) is the Fermi momentum of the electron (hole) pocket. In this way the ordering temperature can be tuned to zero, leading to a QCP. The mismatch parameter  $\delta$  parametrizes the pressure or doping, since both are able to modify the Fermi momenta of the pockets. The QCP gives rise to the desired NFL properties.<sup>10,13,21,22</sup>

The above two pocket model yields superconductivity for  $W < 0$ . An extension of the model to include the transfer of pairs of electrons between the pockets is able to generate superconductivity for  $W > 0$ .<sup>23</sup> This process is of the Umklapp type and requires the additional assumption that  $2\mathbf{Q}$  is equal to a vector of the reciprocal lattice. This model has been studied for a cylindrical Fermi surface by Chubukov, Efremov and Eremin<sup>24</sup> in the context of iron-based superconductors. For certain parameters this extension is able to generate a superconductivity dome around the QCP without substantially modifying the NFL properties.<sup>23</sup>

In this paper, we investigate the antiferromagnetic and superconducting responses in the neighborhood of the QCP of the extended model (with pair transfer) for spherical Fermi surfaces and nesting vector  $\mathbf{Q}$  differing from  $\mathbf{G}/2$ , i.e. in the incommensurate case. Four density response functions have to be considered in this case, namely spin and charge density waves with wave vectors  $\mathbf{Q}$  (incommensurate with the lattice) and  $\mathbf{G}/2$  (commensurate), as well as four response functions for superconductivity, namely  $S$ ,  $S^+$  with homogeneous order parameters and the corresponding phases with order parameters modulated by  $\mathbf{G}/2 - \mathbf{Q}$ . The latter two resemble superconductivity of the Fulde-Ferrell-Larkin-Ovchinnikov (FFLO) type,<sup>25</sup> but with the oscillations determined by the deviation from commensuration of  $\mathbf{Q}$  with the lattice rather than tuned by the magnetic field.

The remainder of the paper is organized as follows. In

sect. II we summarize the model and previous results for the commensurate two-pocket model with pair-transfer scattering amplitude. In sect. III we obtain the renormalization group equations for all the interactions and the eight response functions mentioned above. In contrast to the case  $\mathbf{Q} = \mathbf{G}/2$  these equations now have to be integrated numerically. The numerical results for the response functions and the phase diagram are presented in sect. IV. Conclusions follow in sect. V.

## II. THE MODEL AND PREVIOUS RESULTS

A strong repulsive interaction between electrons gives rise to heavy fermion bands. In the spirit of the FL theory, there are weak remaining interactions between the heavy quasi-particles left after the heavy particles are formed. The heavy electron band is described by two pockets, one electron-like and the other one hole-like, separated by a wavevector  $\mathbf{Q}$ <sup>10,13</sup>

$$H_0 = \sum_{\mathbf{k}\sigma} \left[ \epsilon_1(\mathbf{k}) c_{1\mathbf{k}\sigma}^\dagger c_{1\mathbf{k}\sigma} + \epsilon_2(\mathbf{k}) c_{2\mathbf{k}\sigma}^\dagger c_{2\mathbf{k}\sigma} \right], \quad (1)$$

where  $\mathbf{k}$  is measured from the center of each pocket, and assumed to be small compared to the nesting vector  $\mathbf{Q}$ . Both bands are parabolic, have different Fermi momenta and for simplicity we assume that the Fermi velocity (or density of states) is the same for both pockets. The case with different Fermi velocities is discussed in Ref. 23.

The weak remaining interactions between quasi-particles are given by  $H_W + H_V + H_U + H_P$ <sup>10,13,23</sup>

$$H_W = \sum_{\mathbf{k}\mathbf{k}'\mathbf{q}\sigma\sigma'j=1,2} W_j(\mathbf{q}) c_{j\mathbf{k}\sigma}^\dagger c_{j\mathbf{k}+\mathbf{q}\sigma} c_{j\mathbf{k}'-\mathbf{q}\sigma'}^\dagger c_{j\mathbf{k}'\sigma'} \quad (2)$$

$$H_V = \sum_{\mathbf{k}\mathbf{k}'\mathbf{q}\sigma\sigma'} V(\mathbf{q}) c_{1\mathbf{k}+\mathbf{q}\sigma}^\dagger c_{1\mathbf{k}\sigma} c_{2\mathbf{k}'-\mathbf{q}\sigma'}^\dagger c_{2\mathbf{k}'\sigma'} \quad (3)$$

$$H_U = U(\mathbf{Q}) \sum_{\mathbf{k}\mathbf{k}'\mathbf{q}\sigma\sigma'} c_{1\mathbf{k}+\mathbf{q}\sigma}^\dagger c_{2\mathbf{k}'-\mathbf{q}\sigma'}^\dagger c_{1\mathbf{k}\sigma'} c_{2\mathbf{k}'\sigma} \quad (4)$$

$$H_P = P \sum_{\mathbf{k}\mathbf{k}'\mathbf{q}\sigma\sigma'} \left[ c_{1\mathbf{k}+\mathbf{q}\sigma}^\dagger c_{1\mathbf{k}'-\mathbf{q}\sigma'}^\dagger c_{2\mathbf{k}+\mathbf{p}^*\sigma} c_{2\mathbf{k}+\mathbf{p}^*\sigma} + H.c. \right]. \quad (5)$$

Here  $W$  is the interaction for particles within the same pocket (for simplicity we consider  $W_1 = W_2 = W$ ),  $V$  represents the interaction strength for small momentum transfer between the pockets ( $|\mathbf{q}| \ll |\mathbf{Q}|$ ),  $U$  corresponds to a momentum transfer of the order of  $\mathbf{Q}$ , and  $P$  refers to a process transferring two particles between the pockets, i.e. the number of particles per pocket is no longer conserved. The limit of the Hubbard model (on-site repulsion for electrons with opposite spin) is obtained by choosing  $W_1 = W_2 = V = U = P$ .

Here  $\mathbf{p}^* = \mathbf{Q} - \mathbf{G}/2$  is the vector necessary for the momentum conservation in the  $H_P$  interaction. The momentum is automatically conserved for the remaining three scattering amplitudes. For the commensurate

case  $p^* = 0$ , i.e. the Umklapp condition is satisfied in the scattering process  $H_P$ .<sup>24</sup> In the incommensurate case necessarily  $p^* \neq 0$ , which restricts the phase space in the scattering process for the transfer of a pair of particles between the pockets. Similarly, the Fermi surface mismatch reduces the efficiency of the particle transfer between pockets. When  $k_{F1} = k_{F2}$  there are no restrictions on the phase space for the transfer and the scattering amplitude  $P$  is maximum. Relaxing of this condition reduces the probability for the pair transfer and hence the amplitude  $P$  should decrease with the Fermi surface mismatch  $\delta$ . We can expand the amplitude  $P$  in powers of  $\delta$  and write  $P(\delta) = P(0) - a_1\delta - \frac{1}{2}a_2\delta^2$ , where  $a_1, a_2 > 0$ , since the mismatch should suppress this scattering amplitude. The dependence of the other interaction amplitudes on  $\delta$  is expected to be much weaker because they conserve the number of particles in each pocket and can be neglected.

The renormalization group equations for the commensurate situation ( $\mathbf{Q} = \mathbf{G}/2$ ) can be integrated analytically and yield for the vertices

$$v \pm p_a = \frac{v_0 \pm p_{a0}}{1 - (v_0 \pm p_{a0})\xi_1}, \quad (6)$$

$$w \pm p_c = \frac{w_0 \pm p_{c0}}{1 + (w_0 \pm p_{c0})\xi_0}, \quad (7)$$

$$(v - 2u) \pm (p_a - 2p_b) = \frac{(v_0 - 2u_0) \pm (p_{a0} - 2p_{b0})}{1 - [(v_0 - 2u_0) \pm (p_{a0} - 2p_{b0})]\xi_1}. \quad (8)$$

Here  $w = W\rho_F$ ,  $v = V\rho_F$ ,  $u = U\rho_F$ ,  $p_a = \rho_F P_a$ ,  $p_b = \rho_F P_b$  and  $p_c = \rho_F P_c$  are dimensionless vertices and  $\rho_F$  is the density of states (assumed to be equal for both pockets). The subindex 0 indicates the initial value of the interaction before renormalization. The logarithmic scaling variable is  $\xi$ . For perfect nesting the renormalization continues until either  $\xi$  tends to infinity or a vertex diverges. For mismatched Fermi surfaces the integration of Eqs. (6) and (8) has to be stopped when the Fermi surface mismatch  $\delta$  is reached. Similarly, the external energy and the smearing of the Fermi surface by the temperature have to be taken into account, so that the renormalization ends when  $\xi_1 = \ln[D/(|\omega| + 2T + \delta)]$  unless a vertex diverges earlier. Here  $D$  is the energy cutoff. The Cooper channel, Eq. (7), only involves particles within the same pocket and hence the Fermi surface mismatch does not play any role and the renormalization continues until  $\xi_0 = \ln[D/(|\omega| + 2T)]$ .

Note that each vertex diagram has four legs, two incoming with momenta  $k_1$  and  $k_2$  and two outgoing with  $k_3$  and  $k_4$ . In analogy to parquet equations, the logarithmic dependence of  $P$  can occur in three channels, namely, the zero sound channel ( $k_1, k_4$ ), the so-called third channel ( $k_1, k_3$ ) and the Cooper channel ( $k_1, k_2$ ). In Eqs. (6 - 8) we have denoted these channels as  $P_a$ ,  $P_b$  and  $P_c$ , respectively.

There are six interaction vertices, which in principle correspond to six order parameters. The most impor-

tant forms of order correspond to (i) SDW, (ii) CDW, (iii) two for superconductivity, and (iv) two additional ones, which correspond to alternate SDW and CDW operators.<sup>26</sup> The latter ones are of no relevance to the present paper and will be ignored. The relevant four operators are

$$\mathcal{O}_{SDW} = \sum_{\mathbf{k}} \left( c_{1\mathbf{k}\uparrow}^\dagger c_{2\mathbf{k}\uparrow} - c_{1\mathbf{k}\downarrow}^\dagger c_{2\mathbf{k}\downarrow} \right), \quad (9)$$

$$\mathcal{O}_{CDW} = \sum_{\mathbf{k}} \left( c_{1\mathbf{k}\uparrow}^\dagger c_{2\mathbf{k}\uparrow} + c_{1\mathbf{k}\downarrow}^\dagger c_{2\mathbf{k}\downarrow} \right), \quad (10)$$

$$\mathcal{O}_S = \sum_{\mathbf{k}} \left( c_{1\mathbf{k}\uparrow}^\dagger c_{1-\mathbf{k}\downarrow}^\dagger + c_{2\mathbf{k}\uparrow}^\dagger c_{2-\mathbf{k}\downarrow}^\dagger \right), \quad (11)$$

$$\mathcal{O}_{S^+} = \sum_{\mathbf{k}} \left( c_{1\mathbf{k}\uparrow}^\dagger c_{1-\mathbf{k}\downarrow}^\dagger - c_{2\mathbf{k}\uparrow}^\dagger c_{2-\mathbf{k}\downarrow}^\dagger \right). \quad (12)$$

The respective susceptibilities, obtained by joining the legs of the vertices giving rise to bubble diagrams, are

$$\chi_{SDW}(\mathbf{Q}, \omega) = 2\xi_1 \rho_F \frac{v(\xi_1) + p_a(\xi_1)}{v_0 + p_{a0}}, \quad (13)$$

$$\chi_{CDW}(\mathbf{Q}, \omega) = 2\xi_1 \rho_F \frac{v(\xi_1) - 2u(\xi_1) + p_a(\xi_1) - 2p_b(\xi_1)}{v_0 - 2u_0 + p_{a0} - 2p_{b0}}, \quad (14)$$

where  $\xi_1$  depends on the Fermi surface mismatch  $\delta$ , and

$$\chi_S(\mathbf{Q}, \omega) = 2\xi_0 \rho_F \frac{w(\xi_0) + p_c(\xi_0)}{w_0 + p_{c0}}, \quad (15)$$

$$\chi_{S^+}(\mathbf{Q}, \omega) = 2\xi_0 \rho_F \frac{w(\xi_0) - p_c(\xi_0)}{w_0 - p_{c0}}, \quad (16)$$

where again  $\xi_0$  does not contain  $\delta$ . For  $\delta \rightarrow 0$  these equations have been obtained previously by Chubukov<sup>26</sup> for cylindrical Fermi surfaces in the context of Fe-based superconductors. The results are only based on the nesting condition and are not influenced by the dimension of the problem. The response functions are closely related to the corresponding vertices.

A divergent response function indicates strong coupling and signals an instability. For a repulsive Hubbard-like interaction  $\chi_{SDW}$  displays a divergence and a spin density wave is possible with a Néel temperature

$$T_N = \frac{1}{2} D \exp\{[-\rho_F(V_0 + P_{a0})]^{-1}\} - \frac{1}{2}\delta = \frac{1}{2}(\delta_0 - \delta). \quad (17)$$

The above relation defines  $\delta_0$  and  $T_N$  has a linear dependence with  $\delta$ . The condition for a QCP is  $T_N = 0$  which is reached for  $\delta = \delta_0$ , and if  $T_N < 0$  long range order has not developed. Hence, the Fermi surface mismatch suppresses the AF order and for sufficiently large Fermi surface mismatch the renormalization does not lead to a SDW instability.<sup>13</sup> The QCP is an unstable fixed point and can only be reached by perfectly tuning the system.<sup>10</sup>

If  $V_0 - 2U_0 + P_{a0} - 2P_{b0} < 0$  the CDW response function renormalizes to zero, suggesting no CDW long-range order. Similarly, the Cooper channel response function

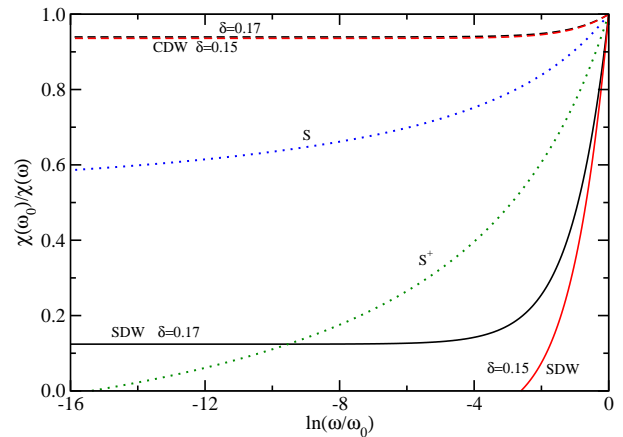


FIG. 1: (color online) Inverse of the correlation functions normalized to their value at  $\omega_0 = 0.1$ . The parameters are  $D = 10$ ,  $w_0 = 0.7$  and  $v_0 = u_0 = p_{a0} = p_{b0} = p_{c0} = 0.12$ . This corresponds to  $\delta_0 = 0.155$  at the QCP. The SDW and CDW curves refer to  $\delta = 0.15$  and  $\delta = 0.17$ .  $\chi_{SDW}$  for  $\delta < \delta_0$  diverges at  $\omega = 2T_N$ . The dependence of the amplitude  $P$  on  $\delta$  has been neglected here. Note the divergence of  $\chi_{S^+}$  at very low energies corresponding to a very small  $T_c$ .

$\chi_S$  also renormalizes to zero, and hence no superconductivity is expected from this channel. However, the  $S^+$  channel has zero effective coupling for  $W_0 = P_{c0}$ . The behavior of this channel then depends delicately on the exact compensation of  $W_0$  by  $P_{c0}$ . If  $P_{c0} - W_0 > 0$  the superconducting transition temperature for the  $S^+$  channel is

$$T_c = \frac{1}{2} D \exp\{[-\rho_F(P_{a0} - W_0)]^{-1}\}. \quad (18)$$

Note that  $T_c$  only depends on  $\delta$  through the pair-transfer amplitude  $P_a$ , which decreases with  $\delta$  and parametrizes the pressure. Let us define  $\delta_s$  such that  $W_0^{(0)} - P_{c0}(\delta_s) = 0$  and assume  $\delta_s > \delta_0$ . Hence, at very low  $T$  there is  $S^+$  superconductivity for  $\delta < \delta_s$  and  $T_c$  gradually increases with decreasing  $\delta$  and eventually gives way to AF close to the QCP at  $\delta_0$ .  $T_c$  is going to cross the SDW boundary given by  $T_N$  and the two forms of order, SDW and  $S^+$ , compete for the same portion of the Fermi surface. A Ginzburg-Landau expansion of the free energy with the two order parameters shows the existence of a mixed phase.<sup>23</sup> Since usually  $T_N(\delta = 0) \gg T_c(\delta = 0)$ , the SDW eventually prevails over the superconductivity giving rise to a dome.

Superconducting domes of this type have been observed in  $\text{CeRh}_2\text{Si}_2$ ,<sup>16,17</sup>  $\text{CePd}_2\text{Si}_2$  and  $\text{CeIn}_3$ ,<sup>18,19</sup> under pressure. Due to the competition between the SDW and the  $S^+$  order the dome is split into two regions, in agreement with NMR experiments for  $\text{CeIn}_3$ ,<sup>27</sup> for  $\text{CeCu}_2(\text{Si}_{0.98}\text{Ge}_{0.02})_2$ ,<sup>28</sup> and  $\text{CeRhIn}_5$ .<sup>29</sup>

The inverse of the correlation functions normalized to their value at  $\omega_0$  is shown in Fig. 1 for a cutoff  $D = 10$ ,  $w_0 = 0.7$  and  $v_0 = u_0 = p_{a0} = p_{b0} = p_{c0} = 0.12$ . This

corresponds to a Fermi surface mismatch parameter at the QCP of  $\delta_0 = 0.155$ . For this figure we neglected the  $\delta$ -dependence of the pair transfer amplitude  $P$ . The two SDW and CDW curves correspond to  $\delta = 0.15$  and  $\delta = 0.17$ , i.e. before and after the QCP. The CDW susceptibility remains finite in either case, but the SDW diverges for  $\delta = 0.15$ . Similarly, the susceptibility for the S-superconducting channel remains finite, while the one of the  $S^+$  channel diverges at a small  $\omega$ . This corresponds to a small superconducting  $T_c$ .

### III. TRANSFER OF PAIRS OF ELECTRONS BETWEEN POCKETS: THE INCOMMENSURATE CASE

So far we have considered the situation where an Umklapp condition between the two pockets, i.e.  $2\mathbf{Q} = \mathbf{G}$ , is satisfied.<sup>24</sup> In this section we extend the calculation to the case  $\mathbf{p}^* = \mathbf{Q} - \mathbf{G}/2 \neq 0$ . The perturbative corrections to the interaction vertices are given by the same diagrams as before, which can be found in Figs. 1 through 3 of Ref. 23. The renormalization equations for the vertices are, however, different, as a consequence of a reduced geometrical phase space due to the finite  $p^*$ .

The effects of  $\delta$  and  $p^*$  are different as shown in Fig. 2. One of the pockets has been translated by  $\mathbf{Q}$ . Hence the spheres are no longer concentric, but the centers are now separated by the vector  $\mathbf{p}^*$ . For the diagram on the left in Fig. 2  $p^*$  is smaller than  $k_{12} = k_{F1} - k_{F2} = 2\delta/v_F$ , while for the sketch on the right  $p^* > k_{12}$ .

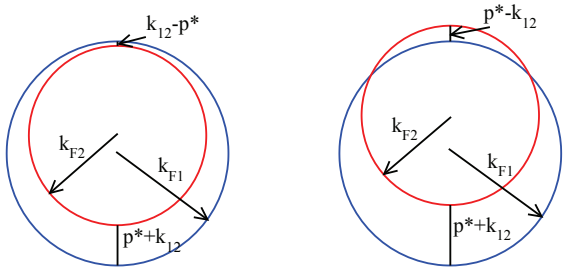


FIG. 2: (color online) Sketch of the Fermi spheres of radius  $k_{F1}$  and  $k_{F2}$  displaced by  $\mathbf{p}^*$ , the incommensurability vector. Here  $k_{12} = k_{F1} - k_{F2}$ . The diagram on the left is for  $p^* < k_{12} = 2\delta/v_F$  and the one on the right for  $p^* > k_{12}$ .

As an example we consider the contribution of order  $p_a^2$  to the small-momentum transfer interaction  $v$ , given by Fig. 2(a) in Ref. 23. The diagram corresponds to a bubble diagram with antiparallel lines of one electron and one hole propagator and hence involves the Fermi surface mismatch  $\delta$ . But the interactions  $P_a$  also involve the momentum  $\mathbf{p}^*$  to ensure momentum conservation. The contribution is proportional to

$$\int \frac{d\omega'}{2\pi} \int \frac{d^3k}{(2\pi)^3} \frac{1}{i(\omega + \omega') - \epsilon_1(\mathbf{k} - \mathbf{p}^*)}$$

$$\times \frac{1}{i\omega' + \epsilon_2(\mathbf{k} + \mathbf{p}^*)}, \quad (19)$$

where  $\omega$  is the external energy. To evaluate this integral we assume that  $p^*$  is a sufficiently small quantity to justify a Taylor expansion in powers of  $p^*$ . Using spherical coordinates, odd powers of  $p^*$  vanish identically due to the angular integrations. Hence, the first nonzero contribution is proportional to  $\alpha = p^{*2}/2m$  and we neglect fourth order terms. The overall contribution of the integral is logarithmic in the cutoff and the external frequency and the  $\alpha$ -term can be re-incorporated into this logarithmic dependence, yielding

$$\xi_2 = \frac{1}{2} \ln \left( \frac{D}{|\omega| + 2T + |\delta - 8\alpha/3|} \right) + \frac{1}{2} \ln \left( \frac{D}{|\omega| + 2T + |\delta + 8\alpha/3|} \right). \quad (20)$$

Similarly, the diagrams of Figs. 2(b) and 2(c) of Ref. 23 have only the  $p^*$ -dependence in  $\epsilon_2$  but not in  $\epsilon_1$  and the logarithmic variable is

$$\xi_3 = \frac{1}{2} \ln \left( \frac{D}{|\omega| + 2T + |\delta - 2\alpha/3|} \right) + \frac{1}{2} \ln \left( \frac{D}{|\omega| + 2T + |\delta + 2\alpha/3|} \right). \quad (21)$$

The leading order diagrams for the zero sound channel now yield the renormalization of the interactions  $V$  and  $P_a$

$$dv = v^2 d\xi_1 + p_a^2 d\xi_2, \quad dp_a = 2vp_a d\xi_3. \quad (22)$$

The logarithmic diagrams contributing to the third channel (see Fig. 3 of Ref. 23) yield the scaling equations for  $P_b$  and  $U^{30}$

$$dp_b = 2[p_b v + up_a - 2up_b] d\xi_3, \quad (23)$$

$$du = -2[u^2 - uv] d\xi_1 + 2p_b(p_a - p_b) d\xi_2. \quad (24)$$

The above diagrams depend on the Fermi surface mismatch and the terms involving a pair transfer vertex,  $p_a$  or  $p_b$ , also depend on the parameter  $\alpha$ .

Similarly, the Cooper channel is modified by diagrams with the interaction vertex  $p_c$  and to leading logarithmic order we have

$$dw = -w^2 d\xi_0 - p_c^2 d\xi_4, \quad dp_c = -wp_c(d\xi_0 + d\xi_5), \quad (25)$$

where

$$\xi_4 = \ln \left( \frac{D}{|\omega| + 2T + 8\alpha/3} \right), \quad (26)$$

$$\xi_5 = \ln \left( \frac{D}{|\omega| + 2T + 2\alpha/3} \right). \quad (27)$$

All the diagrams here involve loops with parallel lines referring to the same pocket. Hence,  $\delta$  does not play

a role here. These equations are completely decoupled from Eqs. (22)-(24).

In contrast to the commensurate case, where  $\alpha = 0$  and the differential equations could all be integrated analytically, for the incommensurate situation numerical methods have to be employed.

We now turn to study the possible phases for the incommensurate case. We noted that the vertices for density waves (Eqs. (22)-(24)) completely decouple from the Cooper channel (Eq. (25)). Hence the density wave response can be treated separately from the correlation functions for superconductivity.

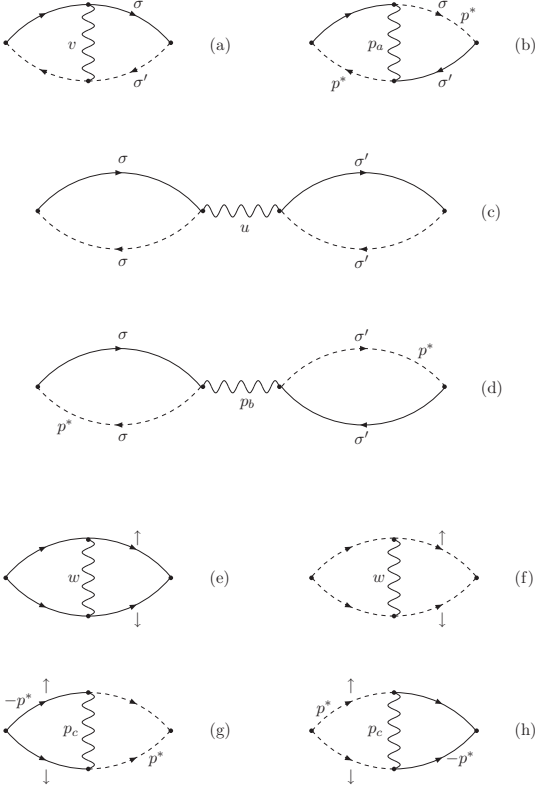


FIG. 3: First-order diagrams contributing logarithmically to the renormalization of the correlation functions. The wavy lines represent one of the six interactions  $v$ ,  $u$ ,  $w$ ,  $p_a$ ,  $p_b$  and  $p_c$ . The solid and dashed lines correspond to propagators for particles in the electron and hole pockets, respectively. Hole propagators that necessarily carry  $\mathbf{p}^*$  are explicitly indicated. Diagram (a) contributes to  $\chi_{SDW}^{inc}$  and to  $\chi_{CDW}^{inc}$ , (b) to  $\chi_{SDW}^{com}$  and to  $\chi_{CDW}^{com}$ , (c) to  $\chi_{CDW}^{inc}$ , (d) to  $\chi_{CDW}^{com}$ , (e) and (f) to  $\chi_S$  and  $\chi_{S^+}$ , as well as to  $\chi_S^{FFLO}$  and  $\chi_{S^+}^{FFLO}$ , but carrying momentum  $\mathbf{p}^*$ , and (g) and (h) to  $\chi_S^{FFLO}$  and  $\chi_{S^+}^{FFLO}$ .

There are two types of possible density waves, namely, commensurate (wavevector  $\mathbf{G}/2$ ) and incommensurate (wavevector  $\mathbf{Q}$ ) with the lattice. The four operators for spin and charge density waves are then

$$\mathcal{O}_{SDW}^{inc}(\mathbf{Q}) = \sum_{\mathbf{k}} \left( c_{1\mathbf{k}\uparrow}^\dagger c_{2\mathbf{k}\uparrow} - c_{1\mathbf{k}\downarrow}^\dagger c_{2\mathbf{k}\downarrow} \right), \quad (28)$$

$$\mathcal{O}_{SDW}^{com}(\mathbf{G}/2) = \sum_{\mathbf{k}} \left( c_{1\mathbf{k}\uparrow}^\dagger c_{2\mathbf{k}+\mathbf{p}^*\uparrow} - c_{1\mathbf{k}\downarrow}^\dagger c_{2\mathbf{k}+\mathbf{p}^*\downarrow} \right), \quad (29)$$

$$\mathcal{O}_{CDW}^{inc}(\mathbf{Q}) = \sum_{\mathbf{k}} \left( c_{1\mathbf{k}\uparrow}^\dagger c_{2\mathbf{k}\uparrow} + c_{1\mathbf{k}\downarrow}^\dagger c_{2\mathbf{k}\downarrow} \right), \quad (30)$$

$$\mathcal{O}_{CDW}^{com}(\mathbf{G}/2) = \sum_{\mathbf{k}} \left( c_{1\mathbf{k}\uparrow}^\dagger c_{2\mathbf{k}+\mathbf{p}^*\uparrow} + c_{1\mathbf{k}\downarrow}^\dagger c_{2\mathbf{k}+\mathbf{p}^*\downarrow} \right), \quad (31)$$

and the first order perturbative corrections to the corresponding susceptibilities are

$$\chi_{SDW}^{inc}(\mathbf{Q}) = 2\rho_F(\xi_1 + v\xi_1^2 + \dots), \quad (32)$$

$$\chi_{SDW}^{com}(\mathbf{G}/2) = 2\rho_F(\xi_3 + p_a\xi_3^2 + \dots), \quad (33)$$

$$\chi_{CDW}^{inc}(\mathbf{Q}) = 2\rho_F(\xi_1 + v\xi_1^2 - 2u\xi_1^2 + \dots), \quad (34)$$

$$\chi_{CDW}^{com}(\mathbf{G}/2) = 2\rho_F(\xi_3 + p_a\xi_3^2 - 2p_b\xi_3^2 + \dots), \quad (35)$$

where the notation is the same as for the vertices. The corresponding diagrams are displayed in Fig. 3.

Due to the fact that the zeroth-order term of these correlation functions has a logarithmic dependence, these susceptibilities do not satisfy the criterion of multiplicative renormalization.<sup>10,31</sup> An auxiliary quantity is introduced,  $\bar{\chi} = (2\rho_F)^{-1}(\partial\chi/\partial\xi)$ , which is normalized to unity at the cutoff energy and satisfies the scaling hypothesis. The renormalization group equations for the susceptibilities are now

$$d \ln \bar{\chi}_{SDW}^{inc}(\mathbf{Q}) = 2vd\xi_1, \quad (36)$$

$$d \ln \bar{\chi}_{SDW}^{com}(\mathbf{G}/2) = 2p_a d\xi_3, \quad (37)$$

$$d \ln \bar{\chi}_{CDW}^{inc}(\mathbf{Q}) = 2(v - 2u)d\xi_1, \quad (38)$$

$$d \ln \bar{\chi}_{CDW}^{com}(\mathbf{G}/2) = 2(p_a - 2p_b)d\xi_3. \quad (39)$$

Once the renormalized vertices are calculated, Eqs. (36)-(39) can be integrated to obtain the auxiliary quantities. An integration of the auxiliary susceptibilities finally yields the desired response functions.

A similar procedure yields the superconductivity responses. Besides the S and S<sup>+</sup> pairings which involve Cooper pairs carrying zero momentum, Cooper pairs with momentum  $\mathbf{p}^*$  are also possible. The latter lead to space modulated order parameters and are analogous to FFLO phases in strong magnetic fields. In this case the period of the space modulation is given by  $\mathbf{p}^*$ . The four relevant operators are given by

$$\mathcal{O}_S = \sum_{\mathbf{k}} \left( c_{1\mathbf{k}\uparrow}^\dagger c_{1-\mathbf{k}\downarrow}^\dagger + c_{2\mathbf{k}\uparrow}^\dagger c_{2-\mathbf{k}\downarrow}^\dagger \right), \quad (40)$$

$$\mathcal{O}_{S^+} = \sum_{\mathbf{k}} \left( c_{1\mathbf{k}\uparrow}^\dagger c_{1-\mathbf{k}\downarrow}^\dagger - c_{2\mathbf{k}\uparrow}^\dagger c_{2-\mathbf{k}\downarrow}^\dagger \right). \quad (41)$$

$$\mathcal{O}_S^{FFLO} = \sum_{\mathbf{k}} \left( c_{1\mathbf{k}+\mathbf{p}^*\uparrow}^\dagger c_{1-\mathbf{k}\downarrow}^\dagger + c_{2\mathbf{k}+\mathbf{p}^*\uparrow}^\dagger c_{2-\mathbf{k}\downarrow}^\dagger \right), \quad (42)$$

$$\mathcal{O}_{S^+}^{FFLO} = \sum_{\mathbf{k}} \left( c_{1\mathbf{k}+\mathbf{p}^*\uparrow}^\dagger c_{1-\mathbf{k}\downarrow}^\dagger - c_{2\mathbf{k}+\mathbf{p}^*\uparrow}^\dagger c_{2-\mathbf{k}\downarrow}^\dagger \right), \quad (43)$$

and the first order perturbative corrections to the corresponding susceptibilities are

$$\chi_S = 2\rho_F(\xi_0 - w\xi_0^2 + \dots), \quad (44)$$

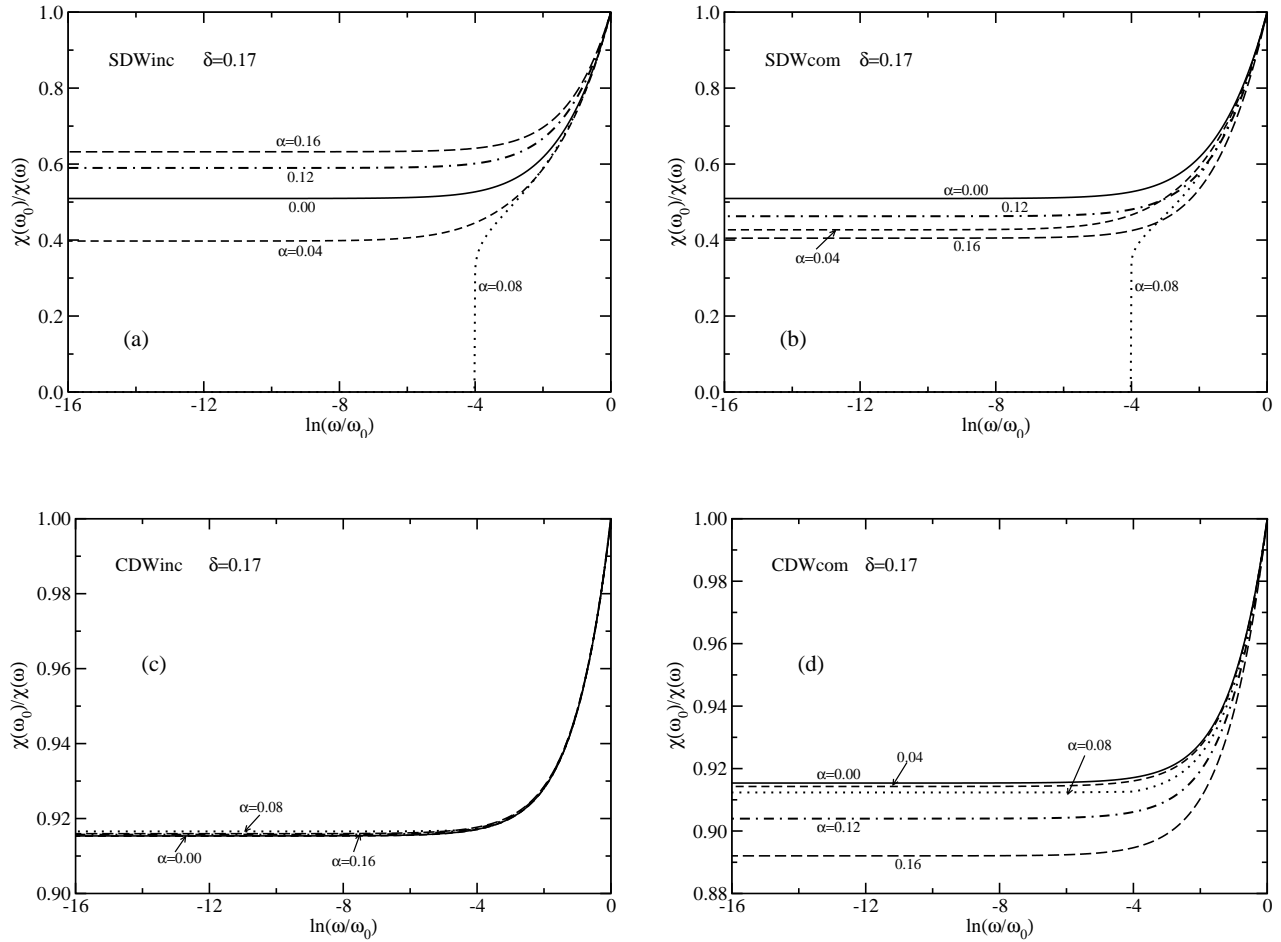


FIG. 4: Inverse of the density correlation functions normalized to their value at  $\omega_0 = 0.1$ . (a) incommensurate SDW, (b) commensurate SDW, (c) incommensurate CDW, and (d) commensurate CDW for  $\delta = 0.17$ ,  $D = 10$ , and  $v_0 = u_0 = p_{a0} = p_{b0} = 0.12$ . The different curves correspond to different values of  $\alpha = p^{*2}/2m$ :  $\alpha = 0$  (solid lines),  $\alpha = 0.04$  (dashed),  $\alpha = 0.08$  (dotted),  $\alpha = 0.12$  (dash-dotted) and  $\alpha = 0.16$  (long-dashed). While the CDW responses remain finite for repulsive interactions, long-range SDW order can be induced for nonzero  $p^*$ .

$$\chi_{S^+} = 2\rho_F(\xi_0 - w\xi_0^2 + \dots), \quad (45)$$

$$\chi_S^{FFLO} = 2\rho_F(\xi_5 - w\xi_5^2 - 2p_c\xi_5^2 + \dots), \quad (46)$$

$$\chi_{S^+}^{FFLO} = 2\rho_F(\xi_5 - w\xi_5^2 + 2p_c\xi_5^2 + \dots). \quad (47)$$

Again, these susceptibilities do not satisfy the criterion of multiplicative renormalization and auxiliary quantities need to be defined. These auxiliary correlation functions,  $\bar{\chi}$ , satisfy scaling and the corresponding differential equations are

$$d \ln \bar{\chi}_S = -2w d\xi_0, \quad (48)$$

$$d \ln \bar{\chi}_{S^+} = -2w d\xi_0, \quad (49)$$

$$d \ln \bar{\chi}_S^{FFLO} = -2(w + p_c) d\xi_5, \quad (50)$$

$$d \ln \bar{\chi}_{S^+}^{FFLO} = -2(w - p_c) d\xi_5. \quad (51)$$

The differential equations need to be integrated numerically to obtain the auxiliary quantities and a second integration yields the actual susceptibilities. A trapezoidal

rule integration with a sufficiently dense distribution of points works quite well.

Note that the vertex functions for the commensurate case can be obtained from the incommensurate situation in the limit  $p^* \rightarrow 0$ . However, the scaling equations for the susceptibilities are different and the commensurate case cannot be recovered as  $p^* \rightarrow 0$ .

#### IV. NUMERICAL RESULTS

The numerical integration of the above differential equations is actually straightforward but quite tedious because some of the vertex functions grow rapidly under renormalization. To obtain the correlation functions requires three nested integrations, which have to be performed with careful accuracy checks. Since for the charge and spin density waves there are commensurate and incommensurate response functions, the susceptibilities are

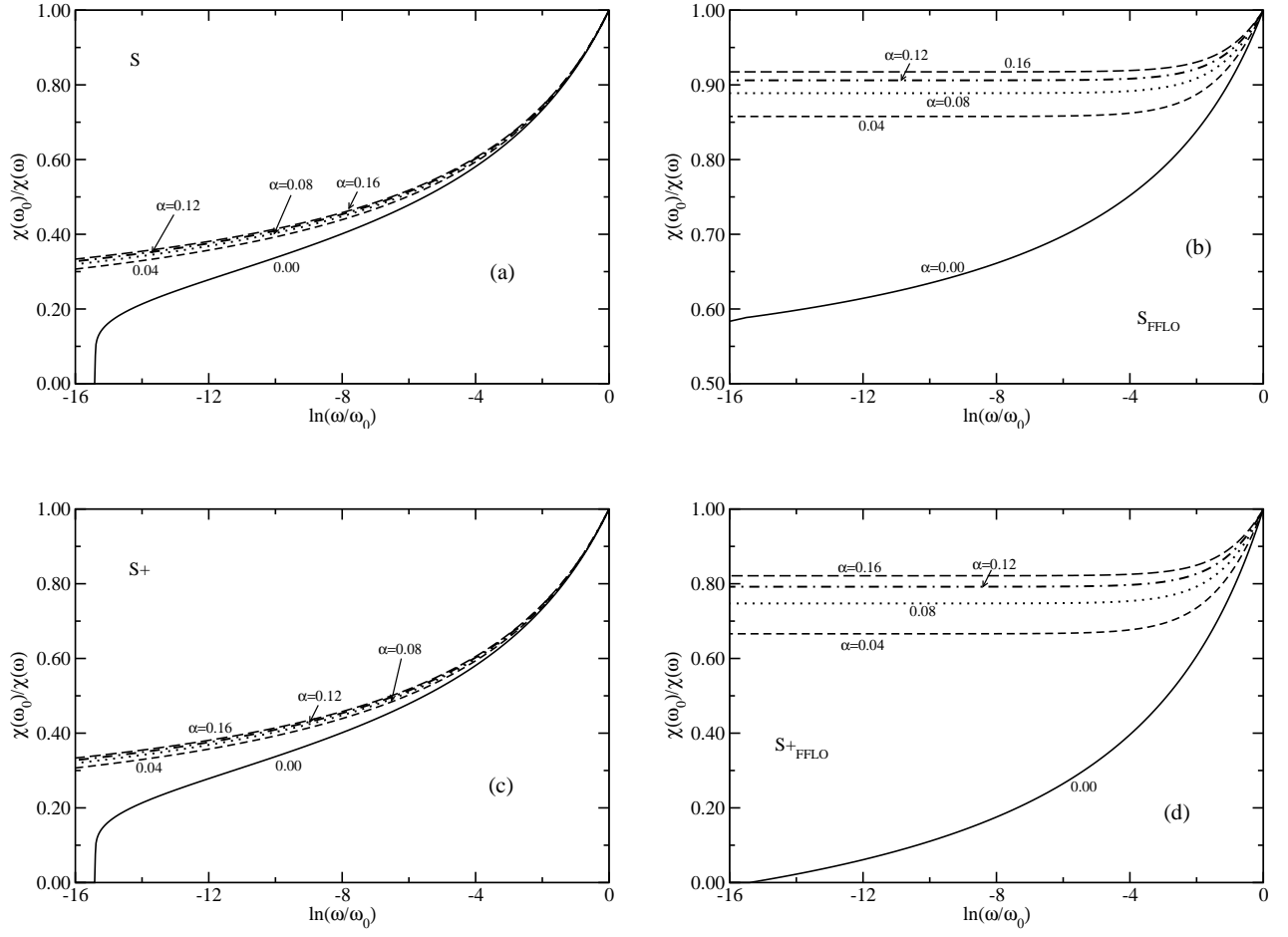


FIG. 5: Inverse of the superconductivity correlation functions normalized to their value at  $\omega_0 = 0.1$ . The type of order is defined by the operators in Eqs. (40) - (43): (a) S-pairing, (b) S-pairing modulated by  $\mathbf{p}^*$ , (c)  $S^+$ -pairing, and (d)  $S^+$ -pairing modulated by  $\mathbf{p}^*$  for  $D = 10$ ,  $w_0 = 0.7$  and  $p_{c0} = 0.12$ . The various curves correspond to different values of  $\alpha = p^{*2}/2m$ :  $\alpha = 0$  (solid lines),  $\alpha = 0.04$  (dashed),  $\alpha = 0.08$  (dotted),  $\alpha = 0.12$  (dash-dotted) and  $\alpha = 0.16$  (long-dashed). Superconductivity is suppressed by  $\alpha$  and only can occur if  $\alpha < T_c$ . Here the dependence of  $p_{c0}$  on  $\delta$  has been ignored.

different than for the commensurate  $\alpha = 0$  case, and the limit  $\alpha \rightarrow 0$  does not have physical meaning.

The inverse of the density correlation functions normalized to their value at  $\omega_0 = 0.1$  is shown in Fig. 4 for various values of  $\alpha$ . The incommensurate and commensurate spin-density waves (Fig. 4(a) and 4(b), respectively) are driven by the vertices  $v$  and  $p_a$ , respectively. For  $\alpha = 0$  both vertices grow rapidly under renormalization and eventually saturate if  $\delta > \delta_0$ , which is the case in Fig. 4. With increasing  $\alpha$ , the logarithmic variable  $\xi_2$  increases because  $\delta$  is compensated by  $\alpha$  in one of the terms. Hence, for small  $\alpha$  and the parameters for Fig. 4, no SDW instability is to be expected. This changes with increasing  $\alpha$  and for  $\alpha = 0.08$  the figure shows a divergence of both,  $\chi_{SDW}^{inc}$  and  $\chi_{SDW}^{com}$ . Further increases of  $\alpha$  take the system back to finite susceptibilities. On the other hand, due to the repulsive nature of the interactions there are no CDW instabilities (Figs. 4(c) and 4(d)).

Fig. 5 displays the responses for the four possible forms of superconducting order. The dependence on  $\delta$  is only through  $p_{c0}$  and has been neglected here. From Eqs. (48) - (51) it is evident that  $\alpha$  is detrimental to superconductivity. Indeed, none of the four phases is favored at sufficiently large  $\alpha$ . For zero- $\alpha$  three of the response functions diverge at a low but finite frequency and the critical temperature is given by Eq. (18). The largest correlation function is  $\chi_{S^+}^{FFLO}$  and this is then the most likely form of long-range order.

In Fig. 6 we show the SDW boundaries for the ground state phase diagram for  $\delta$  vs.  $\alpha$ . The remaining parameters are the same as in Fig. 4. For  $\delta > \delta_0$  with increasing  $\alpha$  we first have Pauli paramagnetism and Fermi liquid behavior, then due to the compensation of  $\delta$  by  $\alpha$  in  $\xi_2$  a SDW arises while  $|\delta - 8\alpha/3|$  is sufficiently small. For larger  $\alpha$  the system returns to a paramagnetic phase but with NFL character. Note that the instability is with respect to both SDW order, commensurate (wavevector

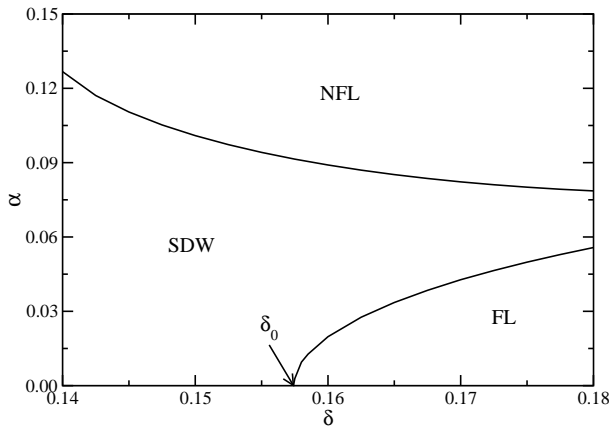


FIG. 6: Ground state phase diagram for  $\alpha = p^{*2}/2m$  as a function of  $\delta$  displaying the SDW phase and the Fermi liquid and NFL regions. The arrow points to the QCP for  $\alpha = 0$  at  $\delta_0$ . The parameters are  $D = 10$ ,  $w_0 = 0.7$  and  $v_0 = u_0 = p_{a0} = p_{b0} = p_{c0} = 0.12$ . Both, commensurate and incommensurate, SDW correlation functions diverge at the same boundary. Superconductivity is suppressed by  $\alpha$  and only can occur if  $\alpha < T_c$ . For the present parameters this essentially corresponds to the  $\alpha = 0$  line on the figure. The  $\delta$ -dependence of the pair transfer amplitudes has been neglected here.

$\mathbf{G}/2$ ) and incommensurate (wavevector  $\mathbf{Q}$ ) with the lattice, since they are both driven by the coupled vertices  $v$  and  $p_a$ . The SDW order could then have either form or even be a superposition of both. At the lower boundary for  $\delta > \delta_0$  the incommensurate SDW susceptibility is slightly larger.

For  $\delta < \delta_0$ , on the other hand, the system is unstable to SDW even for small  $\alpha$ . With increasing  $\alpha$  the order is eventually suppressed and the system becomes a NFL Pauli paramagnet (see Fig. 6). At the phase boundary the commensurate response is several orders of magnitude larger than the incommensurate one. Hence, a SDW with wavevector  $\mathbf{G}/2$  dominates the phase in that parameter regime.

The origin of the compensation of  $\delta$  by  $\alpha$  in  $\xi_2$  through the term with  $|\delta - 8\alpha/3|$  is the following.  $\delta$  represents the Fermi surface mismatch due to concentric (after translating one pocket by  $\mathbf{Q}$ ) spheres. A non-zero  $\mathbf{p}^*$  corresponds to a translation in reciprocal space that leaves the spheres non-concentric. There is then a shortest and largest distance between the spheres, which in terms of energies corresponds to  $|\delta - 8\alpha/3|$  and  $\delta + 8\alpha/3$ , respectively. For  $\xi_3$  only one propagator is shifted leading to a smaller energy adjustment. This is schematically shown in Fig. 2.

Fig. 7 displays the Néel temperature,  $T_N$ , as a function of  $\alpha$  for various parameter values  $\delta$ . For a given  $\delta$ ,  $T_N$  has a cusp when  $\alpha = 3\delta/8$ . For  $\delta > \delta_0$  no SDW order is found for small  $\alpha$ . Increasing  $\alpha$  induces long-range order and  $T_N$  increases, passes through a maximum (cusp) and decreases until the SDW is suppressed. On the other

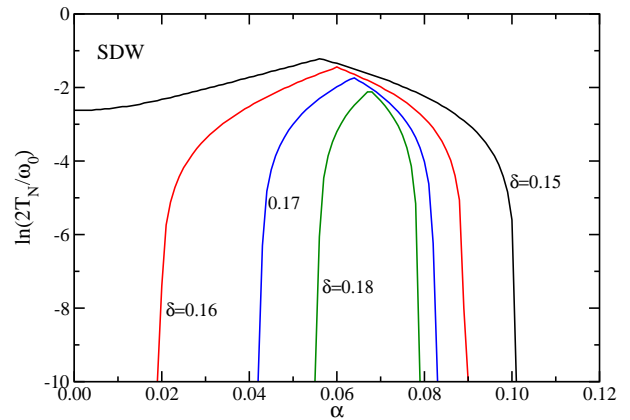


FIG. 7: (color online) Logarithm of the Néel temperature  $T_N$  in units of  $\omega_0 = 0.1$  vs.  $\alpha$  for several values of the Fermi surface mismatch parameter  $\delta$ . The parameters are  $D = 10$  and  $v_0 = u_0 = p_{a0} = p_{b0} = 0.12$ . While there is no CDW instability for repulsive interactions, a SDW instability is induced with increasing  $\alpha$  due to the compensation of  $\delta$  by  $\alpha$  in one of the terms of  $\xi_2$ . For sufficiently large  $\alpha$  the SDW instability is again suppressed. Due to the  $|\delta - 8\alpha/3|$ -dependence there is a cusp in  $T_N$  vs.  $\alpha$ , which corresponds to the zero of the absolute value. If  $\delta < \delta_0$  the SDW extends to  $\alpha = 0$ . The dependence of the amplitude  $P$  on  $\delta$  has been neglected here.

hand, if  $\delta < \delta_0$  the SDW already exists for  $\alpha = 0$  and by increasing  $\alpha$   $T_N$  goes through the cusp and eventually the long-range order is quenched.

## V. CONCLUSIONS

The nesting of a heavy electron Fermi surface can give rise to itinerant AF long-range order. The degree of nesting is controlled by the mismatch parameter  $\delta$  and this way the ordering temperature,  $T_N$ , can be tuned to zero, leading to a QCP. The QCP is an unstable fixed point and can only be reached by perfectly tuning the system. Otherwise, the RG flow will deviate to a phase with long-range order or the compound remains a heavy electron paramagnet. There is no characteristic energy scale associated with the QCP and a small perturbation to the system may give rise to a new physical situation at low energies. This fact is probably responsible for the *lack of universality* in NFL compounds close to the QCP.

We considered the two-pocket model<sup>10,13</sup> including the transfer of pairs of electrons between the pockets<sup>24</sup> and investigated the RG flow in the context of NFL behavior for heavy fermion systems.<sup>23</sup> The pair transfer usually requires the inclusion of Umklapp processes, i.e. a nesting wave vector commensurate with the lattice. Here we studied the situation where the nesting vector  $\mathbf{Q}$  is not commensurate with the lattice, the difference being denoted with  $\mathbf{p}^*$ . This opens the possibility of more forms of long-range order, i.e. commensurate and incommensurate density waves and superconductivity of the FFLO

type, where the modulation of the order parameter is given by  $\mathbf{p}^*$ .

The channels for superconductivity (particle-particle or hole-hole loops) do not depend on the Fermi surface mismatch cutoff, and are completely decoupled from the channels for SDW and CDW (particle-hole loops), which are affected by  $\delta$ . The parameter  $\alpha = p^{*2}/2m$  rapidly suppresses superconductivity, but may induce spin density waves. CDW are in general not favorable with repulsive interactions. For  $\mathbf{p}^* = 0$  the two spherical Fermi surfaces are concentric, once the hole pocket is shifted by  $\mathbf{Q}$ . If  $\mathbf{p}^* \neq 0$  the spheres are no longer concentric and the distance in  $\mathbf{k}$ -space between them is no longer constant, having a maximum and a minimum. This leads to the two terms in the logarithmic variable  $\xi_2$ , one with  $|\delta - 8\alpha/3|$  and the other with  $\delta + 8\alpha/3$ . The former can lead to a SDW instability with both, the incommensurate and commensurate, responses diverging for the same range of parameters  $\delta$  and  $\alpha$  since they are driven by the same coupled diverging vertices.

For fixed  $\alpha$  the AF QCP can be tuned by varying  $\delta$  so that  $T_N \rightarrow 0$ . Here  $\delta$  parametrizes the applied pressure or doping, while  $\alpha$  is determined by the band structure. Pressure affects the band structure of metals and may increase or decrease the energy of the top and bottom of the pockets. Hence, pressure changes  $k_{F1}$  and  $k_{F2}$  with changing the number of electrons and consequently the Fermi surface mismatch parameter  $\delta$ .

The differential equations satisfied by the susceptibilities are different for  $\alpha = 0$  and  $\alpha \neq 0$ . Hence, the limit  $\alpha \rightarrow 0$  is different from  $\alpha = 0$  and not meaningful since the difference between commensurate and incommensurate disappears and the period of modulation of the FFLO phases becomes infinite (all phases are homogeneous). Since superconductivity is only viable for very small  $\alpha$ , the  $\alpha = 0$  equations should be used. This leads to a superconducting phase of the  $S^+$  type with  $T_c$  given by Eq. (18). The  $\delta$ -dependence of  $P_c$  yields a  $\delta_s$

above which  $T_c$  vanishes. If  $\delta_s \gg \delta_0$  a strong superconducting phase is obtained in qualitative agreement with  $\text{CeCu}_2(\text{Si}_{1-x}\text{Ge}_x)_2$ <sup>32</sup> and  $\text{CeMIn}_5$  ( $M = \text{Co}, \text{Rh}, \text{Ir}$ ).<sup>33</sup>

On the other hand, if  $\delta_s$  is only slightly larger than  $\delta_0$  a superconducting dome arises. Superconducting domes of this type have been observed in  $\text{CeRh}_2\text{Si}_2$ ,<sup>16,17</sup>  $\text{CePd}_2\text{Si}_2$  and  $\text{CeIn}_3$ <sup>18,19</sup> under pressure. Due to the competition between the SDW and the  $S^+$  order the dome is split into two regions,<sup>23</sup> in agreement with NMR experiments for  $\text{CeIn}_3$ ,<sup>27</sup> for  $\text{CeCu}_2(\text{Si}_{0.98}\text{Ge}_{0.02})_2$ ,<sup>28</sup> and  $\text{CeRhIn}_5$ .<sup>29</sup>

The results are valid in the disordered phase for weak and intermediate coupling. However, since the renormalization group does not allow a return to a weak-coupling fixed point once the system is strongly coupled, the present approach qualitatively describes the entire precritical regime. Some of the properties are quite universal and independent of the type of QCP. The present model is simple enough so that actual calculations could be performed and may provide insights even for more complex physical situations.

Finally we would like to point out other recent approaches to unconventional superconductivity in heavy fermion systems starting from the Anderson-Kondo lattice models. Bodensiek *et al.*<sup>34</sup> found robust  $s$ -wave superconductivity using the dynamical mean-field theory (DMFT). The DMFT only captures local correlation effects and local spin fluctuations. This result, however, does not exclude other pairings such as  $d$ -waves. Using the so-called statistically consistent renormalized mean-field theory, Howczak *et al.*<sup>35</sup> obtained a phase diagram that includes the coexistence of antiferromagnetism and superconductivity. It would be of interest to learn how fluctuations affect the phase boundaries.

The support by the U.S. Department of Energy under grant DE-FG02-98ER45707 is acknowledged.

<sup>1</sup> H. von Löhneysen, *Physica B* **206 & 207**, 101 (1994).

<sup>2</sup> M.B. Maple, C.L. Seaman, D.A. Gajewski, Y. Dalichaouch, V.B. Barbetta, M.C. de Andrade, H.A. Mook, H.G. Lukefahr, O.O. Bernal, and D.E. MacLaughlin, *J. Low Temp. Phys.* **95**, 225 (1994).

<sup>3</sup> G. R. Stewart, *Rev. Mod. Phys.* **73**, 797 (2001)

<sup>4</sup> H. von Löhneysen, A. Rosch, M. Vojta, and P. Wölfle, *Rev. Mod. Phys.* **79**, 1015 (2007).

<sup>5</sup> B. Andraka and A.M. Tselik, *Phys. Rev. Lett.* **67**, 2886 (1991).

<sup>6</sup> A.M.Tselik and M. Reizer, *Phys. Rev. B* **48**, 9887 (1993).

<sup>7</sup> A.J. Millis, *Phys. Rev. B* **48**, 7183 (1993); J.A. Hertz, *Phys. Rev. B* **14**, 1165 (1976).

<sup>8</sup> M.A. Continentino, *Phys. Rev. B* **47**, 11587 (1993).

<sup>9</sup> T. Moriya and T. Takimoto, *J. Phys. Soc. Jpn.* **64**, 960 (1995).

<sup>10</sup> P. Schlottmann, *Phys. Rev. B* **59**, 12379 (1999).

<sup>11</sup> Q. Si, S. Rabello, K. Ingersent, and J.L. Smith, *Nature*

(London) **413**, 804 (2001).

<sup>12</sup> P. Coleman and C. Pépin, *Physica B* **312-313**, 383 (2002).

<sup>13</sup> P. Schlottmann, *Phys. Rev. B* **68**, 125105 (2003).

<sup>14</sup> J. Custers, P. Gegenwart, H. Wilhelm, K. Neumaier, Y. Tokiwa, O. Trovarelli, C. Geibel, F. Steglich, C. Pépin, and P. Coleman, *Nature (London)* **424**, 524 (2003).

<sup>15</sup> P. Gegenwart, Q. Si, and F. Steglich, *Nature Physics* **4**, 186 (2008).

<sup>16</sup> R. Movshovich, T. Graf, D. Mandrus, J.D. Thompson, J.L. Smith, and Z. Fisk, *Phys. Rev. B* **53** 8241 (1996).

<sup>17</sup> S. Araki, M. Nakashima, R. Settai, T. Kobayashi and Y. Onuki, *J. Phys.: Condens. Matter* **14**, L377 (2002).

<sup>18</sup> I.R. Walker, F.M. Grosche, D.M. Freye, and G.G. Lonzarich, *Physica C* **282-287**, 303 (1997).

<sup>19</sup> N.D. Mathur, F. M. Grosche, S.R. Julian, I.R. Walker, D.M. Freye, R.K.W. Haselwimmer, and G.G. Lonzarich, *Nature (London)* **394**, 39 (1998).

<sup>20</sup> R. Shankar, *Rev. Mod. Phys.* **66**, 129 (1994).

- <sup>21</sup> P. Schlottmann, Phys. Rev. B **73**, 085110 (2006).
- <sup>22</sup> P. Schlottmann, Phys. Rev. B **74**, 235103 (2006).
- <sup>23</sup> P. Schlottmann, Phys. Rev. B **89**, 014511 (2014).
- <sup>24</sup> A.V. Chubukov, D.V. Efremov, and I. Eremin, Phys. Rev. B **78**, 134512 (2008).
- <sup>25</sup> P. Fulde and A. Ferrell, Phys. Rev. **135**, A550 (1964); A. Larkin and Y.N. Ovchinnikov, Zh. Eksp. Teor. Fiz. **47**, 1136 (1964) [Sov. Phys. JETP **20**, 762 (1965)].
- <sup>26</sup> A.V. Chubukov, Physica C **469**, 640 (2009).
- <sup>27</sup> S. Kawasaki, T. Mito, Y. Kawasaki, H. Kotegawa, G.-Q. Zheng, Y. Kitaoka, H. Shishido, S. Araki, R. Settai, and Y. Onuki, J. Phys. Soc. Jpn. **73**, 1647 (2004).
- <sup>28</sup> Y. Kawasaki, K. Ishida, S. Kawasaki, T. Mito, G.-q. Zheng, Y. Kitaoka, Ch. Geibel and F. Steglich, J. Phys. Soc. Jpn. **73**, 194 (2004).
- <sup>29</sup> T. Muramatsu, N. Tateiwa, T.C. Kobayashi, K. Shimizu, K. Amaya, D. Aoki, H. Shishido, Y. Haga and Y. Onuki, J. Phys. Soc. Jpn. **70**, 3362 (2001).
- <sup>30</sup> In Fig. 3(c) and 3(d) of Ref. 23 the vertex should read  $P_a$  (and not  $P_b$ ), while in Fig. 3(e) and 3(f) it should be  $P_b$  rather than  $P_a$ . These typos affect Eq. (23) (the subindices  $a$  and  $b$  have to be interchanged in the last two terms) of Ref. 23, but has no consequence on the remainder of the paper.
- <sup>31</sup> J. Sólyom, J. Low Temp. Phys. **12**, 547 (1973).
- <sup>32</sup> H.Q. Yuan, F.M. Grosche, M. Deppe, C. Geibel, G. Sparn, and F. Steglich, Science **302**, 2104 (2003).
- <sup>33</sup> J.L. Sarrao and J.D. Thompson, J. Phys. Soc. Jpn. **76**, 051013 (2007).
- <sup>34</sup> O. Bodensiek, R. Žitko, M. Vojta, M. Jarrell, and Th. Pruschke, Phys. Rev. Lett. **110**, 146406 (2013); O. Bodensiek, Th. Pruschke, and R. Žitko, IEEE Transactions on Magnetics **50**, 1300205 (2014).
- <sup>35</sup> O. Howczak, J. Kaczmarczyk, and J. Spalek, Phys. Status Solidi B **250**, 609 (2013); O. Howczak and J. Spalek, J. Phys.: Condens. Matter **24**, 205602 (2012).